Journal of Engineering Science and Technology
Vol. 8, No. 4 (2013) 428 - 447

NUMERICAL PREDICTION OF COMPOSITE BEAM SUBJECTED TO COMBINED NEGATIVE BENDING AND AXIAL TENSION

MAHESAN BAVAN, SHAHRIZAN BAHAROM*, AZRUL A. MUTALIB, SITI AMINAH OSMAN

Department of Civil and Structural Engineering, Universiti Kebangsaan Malaysia, Bandar Baru Bangi, Selangor, Malaysia
*Corresponding Author: shah@eng.ukm.my

Abstract

The present study has investigated the finite element method (FEM) techniques of composite beam subjected to combined axial tension and negative bending. The negative bending regions of composite beams are influenced by worsen failures due to various levels of axial tensile loads on steel section especially in the regions near internal supports. Three dimensional solid FEM model was developed to accurately predict the unfavourable phenomenon of cracking of concrete and compression of steel in the negative bending regions of composite beam due to axial tensile loads. The prediction of quasi-static solution was extensively analysed with various deformation speeds and energy stabilities. The FEM model was then validated with existing experimental data. Reasonable agreements were observed between the results of FEM model and experimental analysis in the combination of vertical-axial forces and failure modes on ultimate limit state behaviour. The local failure modes known as shear studs failure, excess yielding on steel beam and crushing on concrete were completely verified by extensive similarity between the numerical and experimental results. Finally, a proper way of modelling techniques for large FEM models by considering uncertainties of material behaviour due to biaxial loadings and complex contact interactions is discussed. Further, the model is suggested for the limit state prediction of composite beam with calibrating necessary degree of the combined axial loads.

Keywords: Composite beam, Tensile forces, Deformation speeds, Energy stabilities, Ultimate state behaviour, Local failures.

1. Introduction

Modern construction industry is being lead in these days by steel-concrete composite structure with the concerns of known aspects cost, bulky and construction methods.

Nomenclatures

E_c	Longitudinal modulus of elasticity of concrete
E_{cm}	Longitudinal modulus of elasticity of concrete
E_s	Elastic modulus of steel
f_{cm}	Compressive strength of concrete
f_{su}	Ultimate stress of steel
f_{sy}	Yield stress of steel
k	Variable in Gattesco Equation
k_s	Constant in Gattesco Equation

Greek Symbols

$\acute{\varepsilon}_c$	Compressive strain of concrete
$\acute{\varepsilon}_{c1}$	Strain at the peak point of concrete
$\acute{\varepsilon}_{cr}$	Strain at concrete cracking
$\acute{\varepsilon}_s$	Strain variables of steel
$\acute{\varepsilon}_{sh}$	Strain at the beginning of hardening stage
$\acute{\varepsilon}_t$	Tensile strain of concrete
σ_c	Compressive stress of concrete
σ_s	Stress variables of steel
σ_t	Tensile stress of concrete

The efficiency of steel-concrete composite beam depends on generating composite action between steel section and concrete slab. Headed shear connectors are key devices as contributing the resistance in the longitudinal shear forces across the steel-concrete interface and as preventing the vertical separation of concrete slab and steel beam**.** Many research studies were in past on the ultimate limit state of composite beam behaviours with either positive or negative bending. But, many real cases reveal that the failure state behaviour in sagging and hogging region will be possible to be occurred as early with the influences of axial tensile loads. The main areas are those that will create axial loads in the steel section such as various cases of machinery links and shafts, elevator and escalator shafts, inclined areas and due to the reasons of non-mechanical forces such as shrinkage and serviceability stresses. In the inclined areas, the enduring bending moment is influenced as a result of combined axial loads and vertical loads. Wind loads are highly effective in tall buildings. It is observed that the beams located accessible on leeward sides are influenced with axial tensile loads and the beams located accessible on windward sides are influenced with axial compressive loads.

There is a lack in proper guidance of design concerns for the failure limit state prediction in the effects of axial loads. There is not existence in any guidelines for an axially loaded composite beam especially in the Eurocode [1]. Meanwhile, limited research studies on the effects of composite beam due to combined axial loads and bending moment are available. The effects of axial tension on the hogging-moment regions of composite beams were investigated with a number of tests by Vasdravellis et al. [2]. They concluded that the negative moment capacity of composite beam is decreased when the level of axial tension is higher and the negative moment capacity is not affected or slightly increased when the axial tension is lower. They concluded further that the partial shear interaction positively contributes the failure state of composite beam by introducing higher ductile levels and by improving the local instability in compression flange.

Vasdravellis et al. [3] continued with six numbers of composite beams to study the effects of axial tension on the sagging-moment regions of composite beams. They reported that the moment capacity is reduced due to the presence of axial tensile forces acting in the steel beam section of composite beam. Vasdravellis et al. [4] studied the behaviour and design of composite beams subjected to negative bending and compression. They made number of conclusions essentially that negative moment capacity of a composite beam is weaken under the simultaneous action of the axial compressive forces.

Steel-concrete composite plate girders subject to combined shear and bending were reported by Baskar and Shanmugam [5]. They found that the effect of the composite action is less in the composite girders subjected to combined shear and negative bending. Nie et al. [6] reported the performance of composite beams under combined bending and torsion and proposed the equation to predict the resistance of steel-concrete composite beams under flexure and torsion. Tan et al. [7, 8] tested a number of straight and curved composite beams to study the effects of torsion and their studies recommended design models for the straight and curved composite beams subjected to combined flexure and torsion. The effects of the combination of axial and shear loading on the headed stud steel anchors were investigated by Mirza et al. [9]. They made conclusions that strength and ductility of composite beam are influenced by nonlinearity of shear connection and the axial tensile capacity is reduced with an increase in slab thickness. Elghazouli and Treadway [10] studied the inelastic behaviour of composite members under combined bending and axial loading. They brought by their analytical studies that the bending moment capacity is influenced by axial load levels with local buckling effects.

Loh et al. [11, 12] presented from a series of tests on the effects of partial shear connection in the hogging moment regions of composite beams. They concluded that the partial and full shear connection beams contain almost similar behaviours and there is slight reduction in ultimate strength with in terms of benefits in ductility. Generally, the unfavourable phenomenon in the compression of steel and concrete cracking may occur in the negative bending regions. Moreover, the axial tensile loads additionally influence the ultimate limit state of composite beams in the negative bending regions and it is observed that the axial loads significantly change the failure mechanism of composite beam near support regions.

In this paper, finite element modelling techniques are analysed to predict more reliable results in the effects of the negative bending regions of a steel-concrete composite beam due to axial loads. There are limited research studies existing on finite element modelling with a solid geometry construction and proper real contact behaviours. Tahmasebinia et al. [13] made report in probabilistic three-dimensional finite element study on composite beam with trapezoidal steel decking about discretizations of meshes in headed shear studs and its influences in results of global behaviours. Qureshi et al. [14] studied the effects of shear connectors spacing and layout on the capacity of shear connectors of a metal-ribbed deck composite beam. Although research studies are available in three-dimensional solid finite element modelling, the prediction of the failure state of composite beam subjected to combined loading has not yet been published. The numerical models are developed with nonlinear spring model for the models of shear connectors in previous studies [2-4] in the effects of combined loadings on

composite beam. Axial load is an essential parameter, which will directly influence early failure by way of excessive slip in the negative regions.

As a result, the most accurate modelling way of solid shear connector was used in these studies based on real contact behaviours linked with the slab and steel beam solid components. Finally, the probable ways of finite element modelling techniques are discussed in this paper based on convergence problems and severe immediate cracking of concrete in the region of surrounding the shear connector. Moreover, finite element modelling is a way to extend to more general cases with various parameters. Based on the numerical studies, the best way of predicting the limit state behaviour of a composite beam with various degrees of combined loadings is suggested in this paper.

2. Experimental Reviews

A number of tests were carried out for steel-concrete composite beam subjected to negative bending and axial tensile loading by Vasdravellis et al. [2]. The test arrangement of composite beam subjected to negative bending and tensile loads is reviewed in Fig. 1(a) and the axial load application method is shown in Fig. 1(b). All composite beams were adopted with a steel section of 200UB29.8 and with a 6oomm-wide and 120 mm-deep reinforced concrete slab. The concrete slab was reinforced by 4450 mm-length, 12 mm-diameter bars in longitudinal direction and 550 mm-length, 12 mm-diameter bars in transversal direction. The cross section of composite beam is shown in Fig. 2. Shear studs of 19 mm diameter and 95 mm long were welded in a single line at the centre of the beam with a spacing of 400 mm and specially, a number of three shear studs were welded at the ends of beams to avoid early failure by excessive slip at the ends. The full shear connection was maintained between concrete slab and steel beam in all specimens by providing sufficient numbers of shear studs. Five numbers of fly bracing systems were used in a beam to avoid premature failure by lateral torsional buckling as bottom flange of the beam subjected to compressive forces due to negative moment.

The detailed test set-up with boundary conditions and the location of shear connectors are indicated in Fig. 3. Both axial and vertical loads were applied simultaneously by using load actuators. While vertical load was applied at centre of bottom flange of the steel beam, the axial tensile loads were applied through the pin, which was connected to the steel beam end and located at the plastic centroid. The level of tension was determined with the relevant percentage of axial and vertical load combinations for the purpose of required analysis.

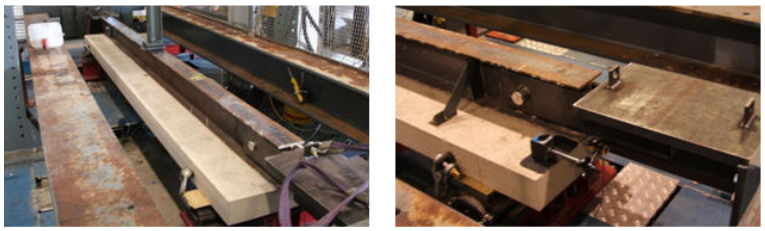

(a) (b)

Fig. 1. (a) Test set up for Negative Bending and Axial Tensile loads (b) Load Applicator to Axial Tensile Loads [2].

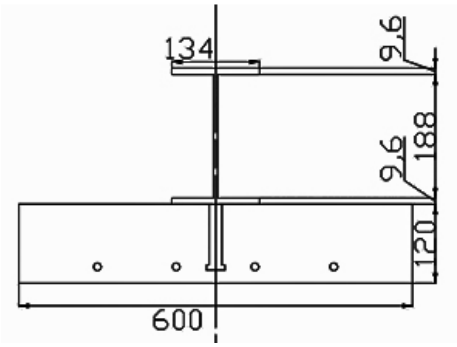

Fig. 2. Composite Beam Cross-Section in Negative Bending and Axial Tensile Loads.

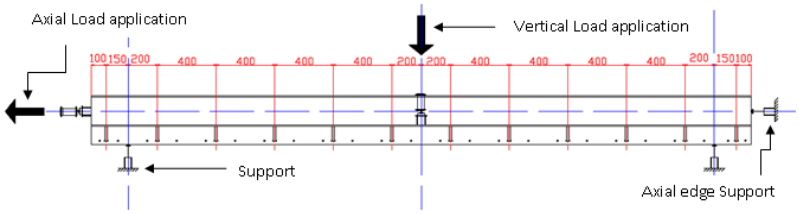

Fig. 3. Details of Test Set-up of Composite Beam Subjected to Negative Bending and Axial Tensile Loads.

The material behaviours were recorded with strain profiles using strain gauges and with connector slip, interface slip and deflection of the beam by using linear potentiometers. Strain gauges were located at middle and quarter intervals of the steel beam by seven numbers in each cross section. Linear potentiometers were placed at the ends, quarters and middle for measuring the connector slip and interface slip and as well, the deflection of the beam was measured by linear potentiometers placed at the quarters and middle. The experimental results were presented with a combination of axial and vertical loads at failure state and mode of failures.

3. Finite Element Analysis

Three dimensional finite element models were developed for analysing the composite beam subjected to the negative bending and axial tensile loads by ABAQUS software with explicit solver. Due to the complex contact interactions, boundary conditions and difficult combined loadings, the static implicit method was encountered convergence difficulties and thus, dynamic explicit method was used. It was found that the dynamic explicit method was more efficient in subjecting of convergence during large deformations, complicated contacts and material failures in the category of combined axial loadings on composite beams.

Half models were developed with considering its symmetries of geometries, boundary conditions and locations of loadings, which was existed in the FEM

model. Though the steel beam and shear studs were developed as one part with considering the welding connections, the concrete slab was developed separately. There are many ways to create the reinforcing bars and the efficiency of results and computational time were considered in modelling. Accordingly, the reinforcing bars were modelled as wire. Half model was then assembled together in proper arrangement like specimens used in experiment.

ABAQUS/Explicit element library has wide range of elements and each element has a unique identification and characteristic performance. ABAQUS manual [15] states that all elements are same in characteristic factors such as element based loads and geometrically nonlinear analysis based on large displacements and rotations. Though any combination of elements is making sensible in its acceptance and the combination of elements was selected with considering its behaviour and computational cost. A continuum, 3D, 8-node reduced integration element (C3D8R) usually provides a solution of equivalent accuracy at less computational cost. By creating proper geometric partitions, C3D8R elements were applied to the concrete slab and solid shear stud models. Continuum, 3D, 8-node incompatible modes (C3D8I) elements were used for the steel beam due to the high concentrated axial load on steel beam. There are several suggested element types in the manual for modelling rebar. The local effects caused by rebars were not important to this study. The results are almost same with different type of elements in the modelling of reinforcing bars and accordingly, truss, 3D, 2 node elements (T3D2) were more reliable on results and computational cost for wire mesh.

The interactions and constraints were decided according to the nature of the deformed body surfaces and the actual characteristic activity of the contact nodes of the deformed body in the experiment. ABAQUS manual [15] suggests in contacting two surfaces that the master surface should be the surface of the stiffer body and the surface containing with coarser mesh. The contact property was defined by tangential behaviour to consider the factors of friction and elastic slip and by normal behaviour to consider the factors of penetration and separation. The surface-to-surface contact algorithm was used to the contact surface between concrete slab and shear stud and concrete slab was selected as master surface. Penalty friction formulation with coefficient of 0.5 was selected to its tangential behaviour and hard pressure over closure was selected to its normal behaviour. In the contact bodies between concrete slab and steel beam, the concrete slab, which was stiffer and contained coarser mesh, was selected as master surface with the same surface-to-surface contact algorithm and contact properties. An embedded region constraint was selected to define the wire mesh nodes. In this constraint, the concrete slab was selected as the host region and the rebar nodes were selected as embedded region as well.

Quasi-static solution is important in ABAQUS explicit solver especially in this static state analysis. Thus, uniform slow load application was needed because of concrete material, which will fail in a sudden deflection and as a result, the static results will evolve to dynamic results owing to speed of the process. In advance, smooth amplitude step was used to acquire more accurate results due to sudden impact load onto the deformed body and to ensure gradual loading during ramping up and down from zero to zero. Both vertical and axial load were applied by displacement method on slab and on surface of the steel beam respectively. In boundary conditions, one end of the steel beam was prevented by translational

movement and various level of axial loads were applied to the other end similarly as experiment**.** The roller supports were modelled by resisting the nodes on the steel beam with a clear span of 4000 mm**.** Details of boundary conditions and load applications are shown in Fig. 4.

The quasi-static analysis is further depending on energy stabilities and it was confirmed by comparing energy balances of kinetic and internal energies of deformed body in this study. Energy balances were maintained throughout the analysis as kinetic energy of deformed model was contained by a small fraction of its internal energy within 5%. Further, the accuracy of results was confirmed by comparing applied and support reaction forces in both directions.

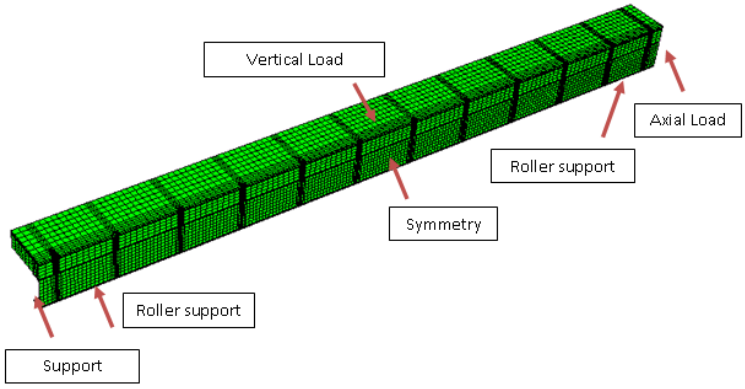

Fig. 4. Boundary Conditions and Load Applications of Developed Finite Element Model.

Concrete is a brittle material and two failure mechanisms are defined as compressive failure and tensile cracking by crushing under compression and cracking under tension respectively. Plastic damage models for concrete are available in ABAQUS with evaluation of yield surface hardening variables proposed by Lubliner et al. [16]. The degradation mechanisms of the hardening variables are characterised in controlling the evolution of failure both under crushing and under tension. Material tests were performed by Vasdravellis et al [2] to each composite beam in the same day of experiments. Kmiecik and Kaminski [17] investigated the strength hypothesis and parameters of concrete. Their studies brought numbers of parameters for concrete biaxial material property such as 36 of dilatation angle, 0.1 of eccentricity, 1.16 of ratio of biaxial and uniaxial state strengths, 0.6667 of ratio of the distance between hydrostatic axis and deviatoric cross section and finally zero value of viscosity. While using the same parameters for biaxial material property of concrete, the compressive and tensile behaviours were developed by using the ultimate limit state values of experiments and with Desayi and Krishnan [18] and Eurocode [19] formulas respectively. The Elastic state of concrete was determined by Eurocode [19] formula as shown in Eq. (1) with value of 0.2 of Poisson's ratio. First 40% of ultimate stress value was assumed as elastic state and the plastic state was developed by Eq. (2) of Desayi and Krishnan [18]. The stress-strain behaviours of concrete in compression and tension are shown in Fig. 5. ABAQUS manual [15]

further suggests the plastic strain will be taken as inelastic strain due to the absence of compression damage and thus compression damage was avoided in the input data in this study. In tensile behaviour, exponential function gives most appropriate results after cracking in fracture energy concept. While elastic behaviour was used with Eq. (3), exponential function was selected to inelastic behaviour with Eq. (4).

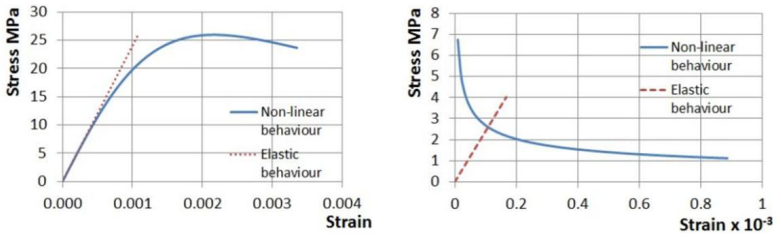

(a) (b)

Fig. 5. (a) Concrete Material in Compression (b) Concrete Material in Tension.

$$E_{cm} = 22(0.1f_{cm})^{0.3} \quad (1)$$

$$\sigma_c = = \frac{E_c \varepsilon_c}{1+\left[\frac{\varepsilon_c}{\varepsilon_{c1}}\right]^2} \quad (2)$$

$$\sigma_t = E_c\, \varepsilon_t \;\; if\; \varepsilon_t \leq \varepsilon_{cr} \quad (3)$$

$$\sigma_t = f_{cm}\left[\frac{\varepsilon_{cr}}{\varepsilon_t}\right]^{0.4} \;\; if\; \varepsilon_t > \varepsilon_{cr} \quad (4)$$

$$\tilde{\varepsilon}_t^{pl} = \tilde{\varepsilon}_t^{ck} - \frac{d_t}{(1-d_t)}\frac{\sigma_t}{E_0} \quad (5)$$

Von Mises yield criterion with isotropic hardening rule (bilinear-hardening material) proposed by Gattesco [20] for large strain analysis was used to model steel beam in this study. The stress-strain graph is shown in Fig. 6. The stress-strain behaviour was divided into three regions as elastic state, perfectly plastic state and nonlinear state with hardening. The elastic state of curve started from origin with positive stress-strain values and the slope of the curve was elastic modulus of the material of steel beam as shown in Eq. (6). It was then perfectly plastic from a specified yield stress f_{sy} as shown in Eq. (7) until beginning of the strain hardening. The curve continued with Eq. (8) until the ultimate stress-strain value, which depends on the steel's ductility. The value of k was defined by Eq. (9) and the value of k_s was 0.028.

$$\sigma_c = E_s\, \varepsilon_s \quad (6)$$

$$\sigma_s = f_{sy} \quad (7)$$

$$\sigma_y = f_{sy} + \left(f_{su} - f_{sy}\right)\left[1 - e^{\left[\frac{(\varepsilon_{sh} - \varepsilon_s)}{k}\right]}\right] \quad (8)$$

$$k = k_x \frac{(\varepsilon_{sh} - \varepsilon_{su})}{(\varepsilon_{sh} - 0.16)} \quad (9)$$

A linearly elastic-perfectly plastic stress-strain curve to material property of shear studs was employed as shown in Fig. 7(a). While the first slope of the curve was taken as the elastic modulus from zero to yield stress of shear studs, the second slope was defined as tangent modulus with value of zero and then, it was started from yield stress-strain values. Material modelling of the reinforcing bars was followed by bilinear stress-strain curve with hardening rule as shown in Fig. 7(b). The initial slope of curve was elastic modulus of material and the curve continued from yield stress with second slope by means of piecewise linear function. In the basis of constitutive law, plastic flow and isotropic hardening were concerned by means of von Mises plasticity.

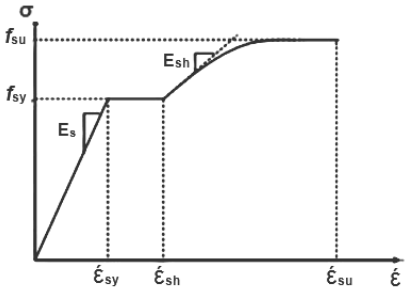

Fig. 6. Stress Strain Curve of Steel Beam.

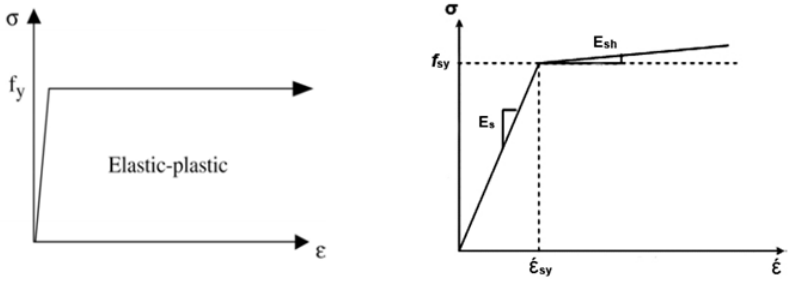

(a) (b)

Fig. 7. (a) Simplified Stress Stain Curve for Shear Studs (b) Stress Stain Curve for Reinforcing Bars.

It is important in ABAQUS explicit solver the analysis of mesh configuration due to the creations of high strain profiles in meshes. In addition, biaxial deformation with non-linear simulations will be characterized in the influences of result by distortion of elements. These sensitive issues should be rectified by minimizing and controlling the distortion of elements for accurate results. Therefore, it was deeply considered in these studies with course, medium and fine meshes to each material component. Six mesh configurations were selected to

concrete slab and steel beam and the studies were made about its margins of errors in the load-deflection responses. Those are (10×10, 10×10), (18×18, 18×18), (50×50, 50×50), (75×75, 75×75), (100×100, 100×100) and (150×150, 150×150), which of mentioned concrete slab and steel beam respectively and named as Mesh type A (finest) to Mesh type F (coarsest). Figures 8(a) to 8(f) are shown the Mesh A to Mesh F.

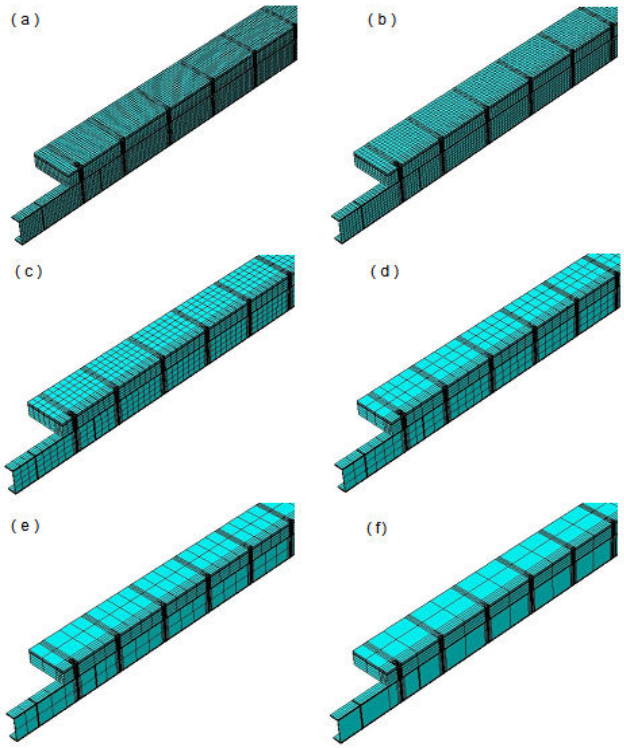

Fig. 8. Mesh Configuration for Concrete Slab and Steel Beam. (a) Mesh type A (10×10, 10×10), (b) Mesh type B (18×18, 18×18), (c) Mesh type C (50×50, 50×50), (d) Mesh type D (75×75, 75×75), (e) Mesh type E (100×100, 100×100), (f) Mesh type F (150×150, 150×150). (Sizes denotes to concrete slab and steel beam respectively.)

Finally, the superlative meshes were selected by evaluating the differences between load-deflection responses and with reasonable computational cost to each material component. Nevertheless adequate results were possible to shear studs with variety of meshes, the shear stud mesh was considered extremely and fine mesh was selected considering with several reasons. Those were mainly that shear studs are a small mechanical device, which will be influenced by high concentrated forces to the meshes of shear studs not only through large shear

forces during transmission between steel beam and concrete slab but also in the course of excess slip by axial loads. The shear stud mesh is shown in Fig. 9.

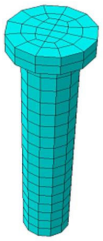

Fig. 9. Mesh Configuration for Shear Stud (5×5).

4. Results and Discussion

A numerical simulation was predicted in this study with considering the similarity of ultimate state behaviour and the stress distribution based on the experimental analysis conducted by Vasdravellis et al. [2]. Explicit solver was used to predict the composite beam behaviour due to the complexity of the contact behaviours and the combined load actions. The control of the explicit solver for prediction of static results was initially studied with various parameters, known as speed and energy stabilities. The proper combination of axial-vertical loads with failure mode of buckling of the compressive flange predicted by the FEM model was validated with experimental results.

Various combinations of deformation speeds directed to negative bending by vertical loads and axial displacement by axial tensile loads were included in these analyses for characteristic reasons. The possibility of failure criteria in materials involving concrete, shear connectors, steel beams and reinforcement was studied with combined vertical-axial loadings. Concrete is a brittle material and thus, it may be suddenly failed in a given sudden change of deformation. In addition, the composite structure was subjected to two different axial deformations in these studies and thus, the deformation speed control was an important factor in both of the axial and vertical axes. Specially, the failure in concrete material had been wanted to control by the deformation of each direction of the loads and it was analysed by stress contour with time increment.

In this numerical model, full degree of shear connection was made. It was confirmed that while applying the monotonic load to negative bending, the structure was reached its limit state capacity with failure mode of buckling in compressive flange. The behaviours of the shear connectors were monitored throughout the analysis to confirm the characteristic behaviour of full shear connection. The benefits of solid elements, which were used for shear connectors for a clear prediction of effects by axial tensile load, were given comprehensible effects as severe immediate cracking of concrete in the regions of surrounding the shear studs. Moreover, the axial load creates the excessive slip in the structure and leads to a significant failure mode by reducing the capacity of the composite beam. Therefore, slow load application was kept throughout the analysis to limit

these failures with quasi-static solution. The deformation speeds of both axes with relevant material behaviour predicted by the FEM model are shown in Fig. 10(a) and (b). Applied load rates of both axial and vertical directions were maintained to avoid improper fluctuation in order to control the material behaviours properly though the displacement control was used. The applied vertical load curve and the applied axial load curve are indicated in Figs. 10(c) and (d) respectively.

The structure behaves with attribute deformation values in spite of given displacement controls. Because of this circumstance in particular deformations at each interval, the loads in each direction were determined with given conditions. Thus, there was a possibility in the loads holding with negative values. However, the static solution of structural capacity was an important component of these studies and as a result, it was maintained throughout the analysis by controlling both axial and vertical load applications with a prediction of simultaneous rises. The gradual increment of vertical load and axial load are shown in Figs. 10(e) and (f).

The total vertical force applied to the specimen was calculated by summing up the reaction forces of nodes in the relevant loading surface of the slab. The axial load was applied on the edge of the steel beam and the applied axial load was calculated by summing up the reaction forces of nodes on the loading surface of steel beam. The proper boundary conditions were applied on steel beam to resist the translational displacements in both axial directions according to the real support conditions. The total reaction forces in the nodes, which were made to resist the vertical deflection with a clear span of 4000 mm, were entirely computed. Similarly, the total reaction forces in the edge of the steel beam, which were made to resist the longitudinal axial displacement, were summed up for evaluating the axial reluctance forces. The applied load and support reaction forces were compared in the basis of both axes to ensure the static equilibrium of the analysis. Comparison the differences between applied loads in vertical and axial directions and the support reaction forces were specified with both axes in Figs. 10(g) and (h). The various levels of speed in both axes were also included in this study with evaluating the uncertainties of the material behaviours to predict the static equilibrium. It was acquired that both applied vertical and axial loads were completely tallied with those particular support reaction forces until reached the relevant combined ultimate limit state values of the vertical and axial loads.

In the explicit solver, it is possible to increase the kinetic energy of the system greatly because of the material failures with sudden drops in the load carrying capacity. Mainly, quasi-static solution is necessary to predict in explicit solver due to the reason that the quasi-static solution limits the kinetic energy of the system to a small value throughout the analysis. It is possible for sudden increase in the kinetic energy compare to internal energy at the initial point even if it was maintained with slow load application. The smooth amplitude function was used for that reason to control the kinetic energy throughout the analysis with proper deformation speeds in both axes. Comparison between kinetic and internal energy is shown in Fig. 10(i) and the percentage difference between kinetic and internal energy is shown in Fig. 10(j). It could be observed that the kinetic energy was possible to be eliminated from the analysis because of its negligible value compared to internal energy.

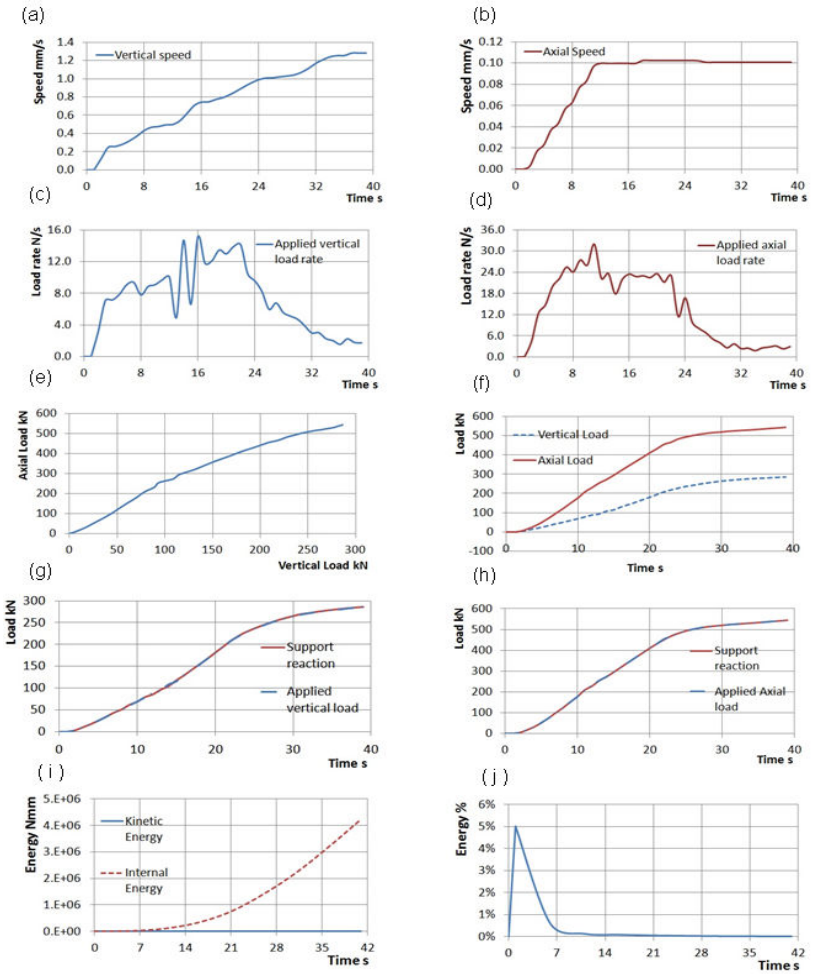

Fig. 10. (a) Vertical Speed along the Axis, (b) Axial Speed along the Axis, (c) Rate of Applied Vertical load Distribution, (d) Rate of Applied Axial Load Distribution, (e) and (f) Comparison between Axial Load and Vertical Load Distributions, (g) and (h) Comparison between Vertical and Axial Applied Load and Support Reaction Force Differences, (i) and (j) Comparison between Kinetic and Internal Energy Differences.

The FEM model after finished with proper deformation speeds was included to convergence studies with different types of meshes. Mesh sizes were determined to each material component and named as Mesh A to Mesh F. The sizes of meshes Mesh A to F were signified as (10x10, 10×10), (18×18, 18×18), (50×50, 50×50), (75×75, 75×75), (100×100, 100×100) and (150×150, 150×150) to concrete and steel beam components. Shear studs were selected with fine mesh (5×5). The predicted results are shown in Figs. 11(a), (b) and (c) as vertical-load deflection curve, axial load-displacement curve and axial load-vertical load curve

respectively. Even as mostly similar results were obtained from axial load-displacement curve and axial load-vertical load curve to all meshes, the mesh A and mesh B only were with comparable similar responses in vertical load-deflection curve. Even though it could be stimulated with mesh A and mesh B, the mesh B was selected for further analysis with majorly considering its computational cost.

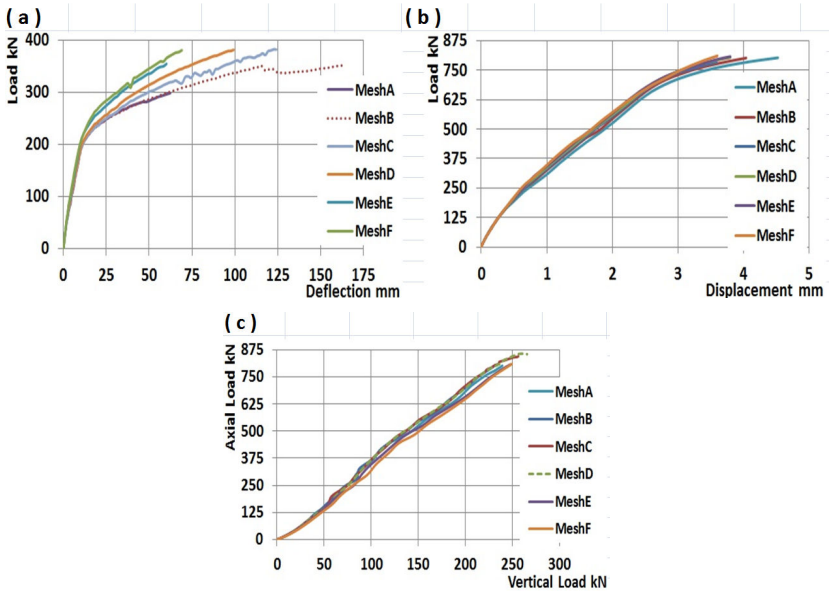

Fig. 11. (a) Vertical-Load Deflection Curve with Various Meshes, (b) Axial Load-Displacement Curve with Various Meshes, (c) Axial Load-Vertical Load Curve with Various Meshes.

In the numerical analysis, the stress-strain profile and slip behaviour in the composite section were monitored throughout the analysis. The vertical load-deflection responses and axial load-axial displacement responses were employed to determine the ultimate load of the composite beam subjected to combined biaxial loads. The vertical load-deflection and axial load-displacement responses of specimen predicted by FEM model are shown in Figs. 11(a) and (b) respectively. The comparison between experiment and numerical analysis in combined axial and vertical loads is shown in Fig. 11(c). The predicted values of vertical and axial loads obtained from FEM analysis were 242.64 kN and 500.34 kN respectively. In the experimental study performed by Vasdravellis et al. [2], the first failure mode of buckling of the compressive flange was observed when the combination of vertical and axial loads values were 263 kN and 460 kN respectively. The similar buckling shape was observed numerically. Good agreement was existed between the numerical model and the experimental data in terms of the ultimate limit state in combined loads and the mode of failure. The combination of loads in ultimate limit

state obtained numerically was deviated with experimental results approximately 7% and 9% of vertical and axial loads respectively.

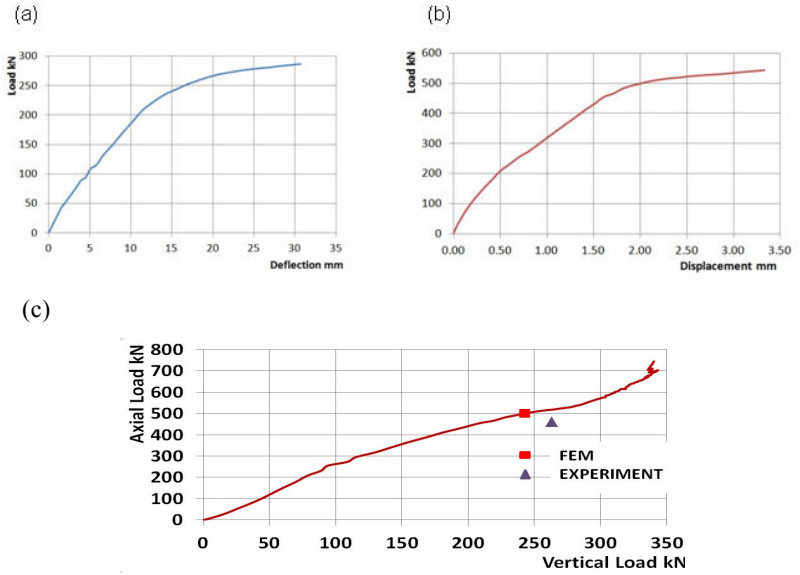

Fig. 12. (a) Vertical Load-Deflection Curve, (b) Axial Load-Displacement Curve, (c) Axial Load-Vertical Load Curve with Comparison between FEM and Experiment.

Due to the combined axial tensile load and negative bending, the compressive behaviour of the steel beam and concrete slab are important to study. The plasticity behaviour of the materials was included in FEM models to study the yielding behaviour of the materials in order to intend the prediction of the failure behaviour of composite beam. The maximum compressive and tensile strains of the concrete material and the maximum tensile strain of the steel beam were analysed at the vertical loading areas of mid-span with simultaneous time increment to predict the failure state in FEM model. The shear connectors were used as mechanical devices to transmit the forces from steel beam to concrete slab in the negative bending region and to avoid the separation between concrete slab and steel beam of the composite beam.

Their behaviour commonly depends on the material behaviour of the composite beam components, which are the compressive strength of the concrete and the tensile strength of steel beam. The slip between concrete slab and steel beam influences the level of axial tension and thus, full shear interaction was considered in this analysis to determine the ultimate limit state of composite beam with combined loads. The developed FEM model was also integrated with monotonic vertical loading applications and it was observed that there was no slip between slab and steel beam throughout the analysis. The stress contour of all material components were studied all over the numerical analysis. Figs. 13(a) to (c) show the yielding region of the compressive flange of steel beam and the Von Mises stress contour of the shear connection area. The highlighted area in

Fig. 13(a) shows that the top of the steel beam flanges and this region was initially initiated the yielding strength. The yielding regions were extended further with increasing axial and vertical loads and the composite beam was shifted to failure state as shown in Fig. 13(b). At the predicted ultimate load, the von Mises stress distribution was shown the yielding region of the steel beam as shown in Fig. 13(c). Figures 14(a) to (c) show that, the peak stress of the steel beam reached the ultimate strain at the mid-span of the compressive flange. It was clear that the similar failure mode of compressive flange buckling was predicted in the FE model as observed in experimental work.

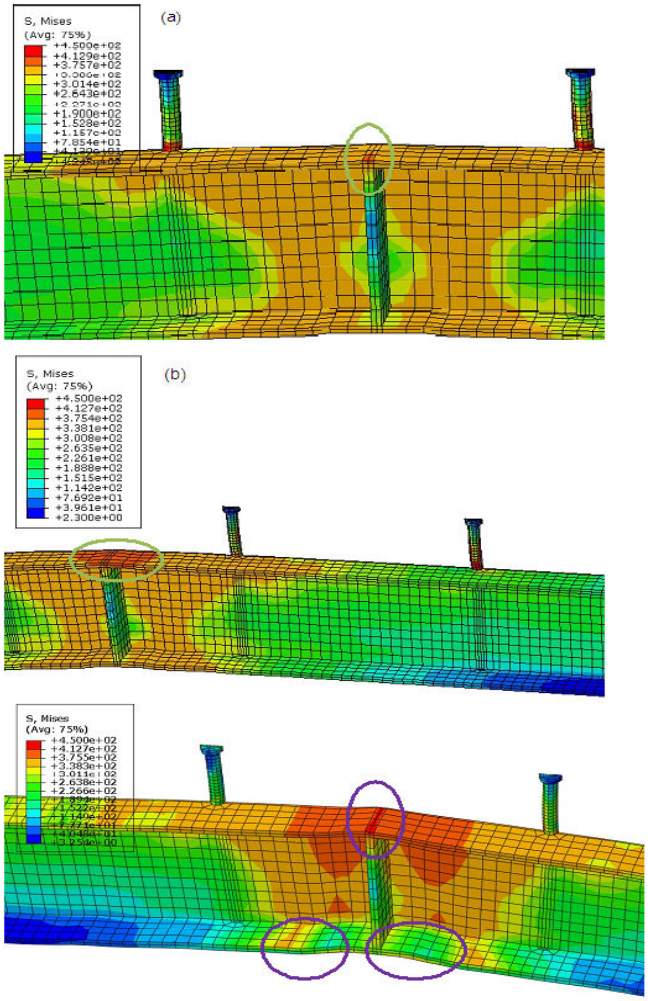

Fig. 13. (a), (b) and (c) Von Mises Stress Contour of Steel Beam Elements at Final Failure Zones in Compressive Flange with Increasing Combined Axial and Vertical Loads.

It should be noted from Figs. 14(a) to (c), the symmetrical local stress distributions were taken in the numerical model. The high stress zones were reached in the shear studs along the axis in the longitudinal direction of the crushing zone of concrete as shown in Fig. 14(c).

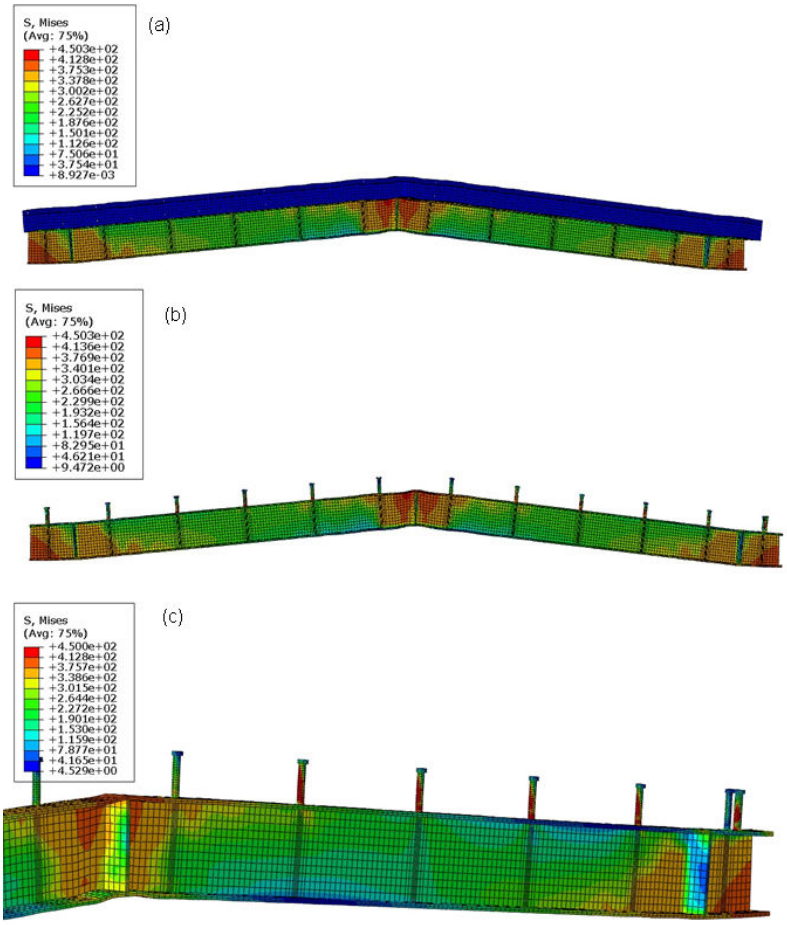

Fig. 14. Full Specimen and the Steel Beam Behaviour at End of Specimen (a) Von Mises Stress Contour of Specimen, (b) Yielding Region, (c) Yielding Region of Compressive Flange.

The concrete failures are shown in Figs. 15(a) and (b) which indicate the concrete cracking elements. The extensive yielding of the composite beam and flange buckling were predicted at the ultimate load. Finally, composite beam was ended with further increases in the loads. In addition, because of the axial tensile load, the stresses were gradually increased in shear connection areas and thus, it was subsequently increased the slip between the concrete and the steel beam. The developed stresses zones on the shear studs are shown in Figs. 16 (a) and (b). The stresses at the mid-span of the steel beam were exceeded the first yielding stress

zone because of the induced compression under global negative bending. The stress zones of each shear studs were exceeded because of the slip induced by the axial tensile loads and negative bending.

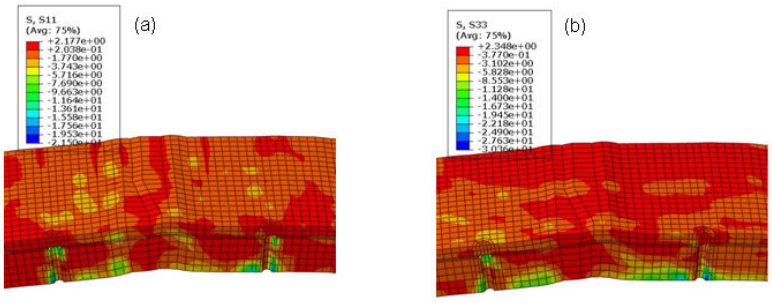

Fig. 15. (a) Transverse Stress Contour of the Concrete and Cracking Elements and (b) Longitudinal Stress Contour of the Concrete.

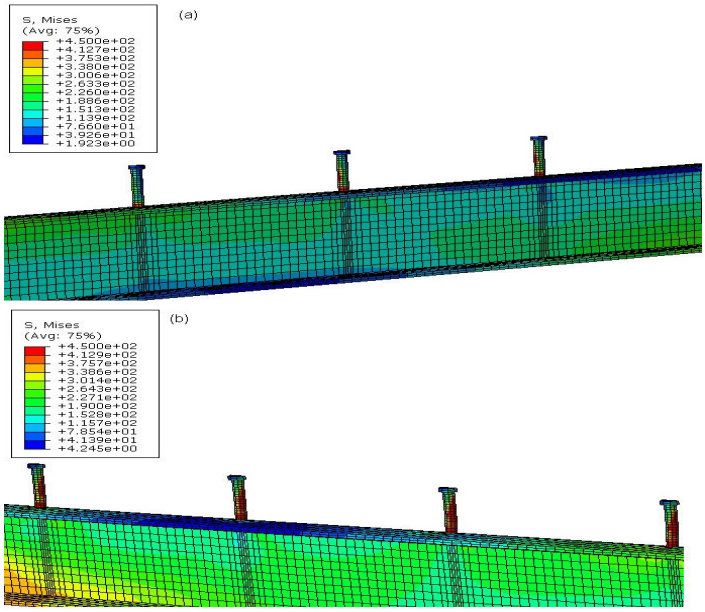

Fig. 16. (a) and (b) Von Mises Stress Contour of Shear Studs Elements with Increasing Combined Axial and Vertical Loads.

5. Conclusions

Three dimensional FEM model was developed to study the effects in behaviour of composite beam subjected to combined vertical and axial tensile loadings. The concrete damage plasticity model and Gattesco [20] nonlinear steel beam model were used to predict the highly nonlinear behaviours of structure. Explicit solver was used due to the complex contact interactions and material nonlinearities. The following conclusions could have been made in this study.

- The FEM model was analysed with various levels of low-velocity impacts in combined axes. The results of the FEM model with various speeds were analysed in basis of element distortion and static state prediction. Best agreement was observed with optimum values of velocities 0.5 mm/s and 1.0mm/s in the applications of vertical and axial tensile loadings respectively.
- The studies were made with discretisations of meshes. It was observed that large strain values were enormously created in meshes in the basis of combined axes loadings with non-linear simulations. The sizes of meshes with geometrical shapes will influence in the numerical results in ABAQUS explicit solver.
- The comparison of the failure modes and ultimate limit state values between FEM model and experiment was brought that the FEM model is reliable. Therefore, this FEM model is applicable for the analysis in underlying mechanisms governing the behaviours of various levels of axial tensile loads on the negative moment region of steel-concrete composite beam. Finally, this FEM model is suggested for the design analysis in postponing the failure of structure subjected to biaxial forces through locally strengthening with stiffness wherever necessary.

These studies generally give the details in the prediction of limit state behaviours of large models with the influences of material uncertainties. Based on unavailability of design codes in various cases, the proposed models can be used by engineers and researchers for various structural analyses, assessment of different combinations of loadings capacities and parametric studies of steel-concrete composite structures. However, more experimental and computational works are still needed to determine the damage types and ultimate limit state behaviour of composite structure in most general manner.

Acknowledgment

The authors wish to thank Universiti Kebangsaan Malaysia (UKM-GGPM- NBT-029-2011 and UKM-GUP-2011-067) for their financial assistance of this research.

References

1. BSI. DD ENV 1994-1-1. EC4: Design of composite steel and concrete structures-Part 1-1: General rules for buildings. London: British Standard Institution.
2. Vasdravellis, G.; Uy, B.; Tan, E.L.; and Kirkland, B. (2012). The effects of axial tension on the Hogging moment region of composite beams. *Journal of Constructional Steel Research,* 68(1), 20-33.
3. Vasdravellis, G.; Uy, B.; Tan, E.L.; and Kirkland, B. (2012). The effects of axial tension on the sagging-moment regions of composite beams. *Journal of Constructional Steel Research*, 72, 240-253.
4. Vasdravellis, G.; Uy, B.; Tan, E.L.; and Kirkland, B. (2012). Behavior and design of composite beams subjected to negative bending and compression. *Journal of Constructional Steel Research*, 79, 34-47.

5. Basker, K.; and Shanmugam, N.E. (2003). Steel concrete composite plate girders subject to combined shear and bending. *Journal of Constructional Steel Research*, 59(4), 531-557.
6. Nie, J.; Luo, L.; and Hu, S. (2000). Experimental study on composite steel-concrete beams under combined bending and torsion. *Composite and Hybrid Structures*, 2, 631-638.
7. Tan, E.L.; and Uy, B. (2009). Experimental study on straight composite beams subjected to combined flexure and torsion. *Journal of Constructional Steel Research,* 65(4), 784-793.
8. Tan, E.L.; and Uy, B. (2009). Experimental study on curved composite beams subjected to combined flexure and torsion. *Journal of Constructional Steel Research,* 65(8-9), 1855-1863.
9. Mirza, O.; and Uy, B. (2010). Effects of the combination of axial and shear loading on the headed stud steel anchors. *Engineering Structures*, 32(1), 93-105.
10. Elghazouli, A.Y.; and Treadway, J. (2008). Inelastic behaviour of composite members under combined bending and axial loading. *Journal of Constructional Steel Research,* 64(9), 1008-1019.
11. Loh, H.Y.; Uy, B.; and Bradford, M.A. (2004). The effects of partial shear connection in the hogging moment regions of composite beams; Part 2-Experimental study. *Journal of Constructional Steel Research*, 60(6), 897-919.
12. Loh, H.Y.; and Uy, B.; and Bradford, M.A. (2004). The effects of partial shear connection in the hogging moment regions of composite beams; Part 1-Analytical study. *Journal of Constructional Steel Research*, 60(6), 921-962.
13. Tahmasebinia, F.; Ranzi, G.; and Zona, A. (2013). Probabilistic three-dimensional finite element study on composite beam with steel trapezoidal decking. *Journal of Constructional Steel Research*, 80, 394-411.
14. Qureshi, J.; Lam, D.; and Ye, J. (2011). Effects of shear connectors spacing and layout on the shear connector capacity in composite beam. *Journal of Constructional Steel Research*, 67(4), 706-719.
15. ABAQUS, User manual, Version 6.9.
16. Lubliner, J.; Oliver, J.; Oller, S.; and Onate, E. (1989). A plastic-damage model for concrete. *International Journal of Solids and Structures*, 25(3), 299-329.
17. Kmiecik, P.; and Kaminski M. (2011). Modelling of reinforced concrete structures and composite structures with concrete strength degradation taken into consideration. *Proceedings of Archives of Civil and Mechanical Engineering VI*, Wroclaw, Poland, 623-636.
18. Desayi, P.; and Krishnan, S. (1999). Equation for the stress-strain curve of concrete. *ACIJ Proceed*, 61(22), 345-350.
19. BSI. DD ENV 1992-1-1. EC2: Design of concrete structures-Part 1-1: General rules for buildings. London: British Standard Institution.
20. Gattesco, N. (1999). Analytical modelling of nonlinear behavior of composite beams with deformable connection. *Journal of Constructional Steel Research*, 52(2), 195-218.